Dynamic Modeling and Trajectory Tracking Controller of a Novel Flying Parallel Robot

Damien Six [*,**] **Abdelhamid Chriette** [*,**] **Sébastien Briot** [*]
Philippe Martinet [*,**]

[*] *IRCCyN, UMR CNRS 6597, France (e-mail: {damien.six, abdelhamid.chriette, sebastien.briot, philippe.martinet}@irccyn.ec-nantes.fr)*
[**] *Ecole Centrale de Nantes, France*

Abstract: This paper presents a new flying robot, composed of two quadrotors linked by a rigid articulated passive chain. The robot obtained is similar to a parallel robot where the classic actuators have been replaced by flying drones. With its rigid structure presenting an internal degree of freedom, the robot presented is a step forward in flying robotics and presents new challenges for the design of its feedback control. In this paper the dynamic modelling of the robot is analyzed. From this analysis, a decoupling property is extracted leading to a cascaded controller based on feedback linearization. An application to trajectory tracking is developed. The effectiveness and robustness against noise in pose estimation of the proposed controller is verified through a realistic simulation.

Keywords: Flying robots; Nonlinear Control; Feedback linearization; Dynamics; Parallel robots

1. INTRODUCTION

The past decade has seen the development of quadrotors Unmanned Aerial Vehicle (UAV) with high performances in constrained environments. They have gained increasing interest in a large panel of applications as observation, surveillance and logistics. Several studies have also explored drone aerial manipulation, through the use of rigid tool attached to the drone (Nguyen et al., 2015a) or serial manipulator associated to one drone as in Yang and Lee (2014); Korpela et al. (2013). Such robots have low payload and, when serial manipulators are used, the additional motors of the arm reduce the energetic autonomy. To overcome those limitations, some studies have explored the collaborative work of several drones associated to a rigid body (Nguyen et al., 2015b; Kim et al., 2014) or cable suspended payload transportation (Manubens et al., 2013; Sreenath and Kumar, 2013). This last configuration can be seen as a cable-driven parallel robot where classic actuators have been replaced by quadrotors. The cables are an appropriate solution to lift a load but, due to the intrinsic characteristics of cables, such structure cannot apply a pushing force on the environment.

This paper explores a new flying structure inspired from rigid parallel robots. Several drones are linked with a rigid articulated passive chain. The flying robot obtained present several advantages over the other explored solutions:

- the ability to perform tasks under but also over the drones, depending of the passive chain configuration,
- the efforts applied on the tool are spread over the drones, enhancing the total payload of the robot,
- the absence of additional embedded motors to actuate the effector reduces the load of the system itself and maintain the energetic autonomy of the drones,

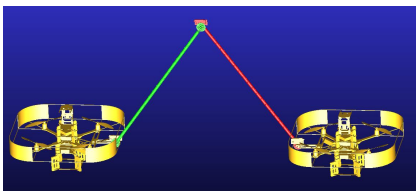

Fig. 1. Snapshot of the flying parallel robot simulator realized with the software ADAMS

- the large choice of leg topology Gogu (2008) leading to a variety of physical properties of potential interest.

Those properties offer interesting potential future applications in maintenance, manipulation and inspection in constrained environments. The paper is structured as follows. A kinematic description of the robot is presented in section 2. In the design of the flying robot, the authors selected quadrotors to lift the structure and perform the actuation (see Fig. 1). This solution was taken on due to the increasing availability of low cost and reliable quadrotors. To the knowledge of the authors, such flying structures have not been already explored and offer new challenges in the design of a feedback control law. In section 3, an analysis of the dynamic model is then performed in order to highlight the possible decouplings to control the underactuated structure. From this analysis, a controller based on cascaded feedback linearization is developed in section 4. The stability of the designed controller is discussed. Simulations are then performed to check the controller performances in section 5.

2. PARAMETRIZATION AND KINEMATIC MODEL

The flying structure is composed of quadrotors, linked by a passive kinematic chain (Fig. 1). The underactuation

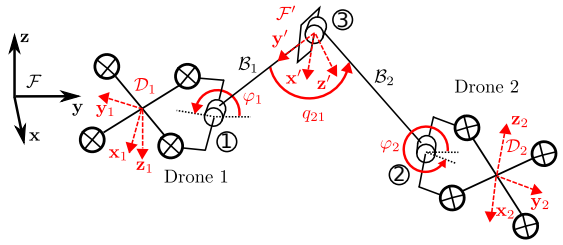

Fig. 2. Parametrisation of the flying parallel robot

of quadrotors combined with the coupling induced by the rigid chain is a new challenge for the modelling and control of the flying robot. To reduce the complexity of the study, the robot is designed to perform motions restricted to a vertical plane. Precautions taken in the control law to maintain the flying structure in this plane are discussed in section 4. The flying robot is then derived from a planar parallel mechanism, the biglide mechanism. This flying robot obtained is composed of two drones (named drone 1 and drone 2) and a two links passive kinematic chain ($\mathcal{B}_1$ and $\mathcal{B}_2$). Revolute joints are selected to constrain the motion of the passive kinematic chain to a planar motion. The passive joints connecting the passive chain to the drone 1 and 2 are respectively named joint ① and ②. The passive joint corresponding to an end-effector in the middle of the passive kinematic chain is named joint ③. Figures 1 and 2 give a general view of the designed structure and its kinematic parameters. The frame $\mathcal{F}$ with axis $\mathbf{x}$, $\mathbf{y}$ and $\mathbf{z}$ is defined as world frame. To describe the position and orientation of the structure in space, a local frame $\mathcal{F}'$ is attached to the end-effector. The orientation of this frame is defined with axis $\mathbf{x}'$ aligned with the passive joint ③ axis and axis $\mathbf{y}'$ aligned with the passive chain link attached to the drone 1. The orientation of the the local frame $\mathcal{F}'$ is parametrized by three successive rotations about $\mathbf{z}$ (Yaw), $\mathbf{y}$ (Pitch) and $\mathbf{x}$ (Roll) axis. The revolute joints limit the internal motions of the structure to a plane orthogonal to the joint axes, the plane spanned by the vectors $\mathbf{x}'$ and $\mathbf{y}'$. The full coordinate vector $\mathbf{q} = [x, y, z, \psi, \theta, \phi, q_{21}, \varphi_1, \varphi_2]^T$ of the flying parallel robot is then composed of

- x, y, z the origin of the local frame $\mathcal{F}'$ expressed in world frame $\mathcal{F}$,
- ψ, θ, ϕ the representation in the global frame $\mathcal{F}$ of the local frame $\mathcal{F}'$ orientation (Yaw/Pitch/Roll angles),
- q_{21} the relative angle between $\mathcal{B}_1$ and $\mathcal{B}_2$,
- φ_1 and φ_2 the roll angle of respectively drone 1 and drone 2.

Two local frames $\mathcal{D}_1$ and $\mathcal{D}_2$ are respectively attached to drone 1 and 2 center. Their respective orientations in the global frame $\mathcal{F}$ are given by (yaw/pitch/roll): $(\psi, \theta, \varphi_1)$ for drone 1, $(\psi, \theta, \varphi_2)$ for drone 2. The drones twists (velocity screws) $\mathbf{t}_1$ and $\mathbf{t}_2$ expressed in local drone frames are related to the coordinate velocities $\dot{\mathbf{q}}$ through the Jacobian matrices $\mathbf{J}_1$ and $\mathbf{J}_2$

$$\begin{bmatrix}\mathbf{t}_1\\ \mathbf{t}_2\end{bmatrix} = \begin{bmatrix}\mathbf{J}_1\\ \mathbf{J}_2\end{bmatrix}\dot{\mathbf{q}} = \mathbf{J}\dot{\mathbf{q}} \tag{1}$$

$\mathbf{J}$ is a (12×9) matrix. The matrix $\mathbf{J}$ is full rank, unless the two passive links of the structure are aligned. In this case, the Jacobian matrix $\mathbf{J}$ becomes rank deficient. Those singularities are the analogue of Type-2 singularities (Gosselin and Angeles, 1990) that appear on the biglide mechanism when the two distal links (equivalents to bodies $\mathcal{B}_1$ and $\mathcal{B}_2$) are aligned. An uncontrolled motion of the effector appears in such singularities. They are not considered in this paper.

As previously said, the mechanism was designed to carry out planar vertical motions. Then, for the study of its dynamics, the robot is considered maintained close to a vertical plane $x = 0, \psi = 0, \theta = 0$. In this vertical plane, the configuration of the passive chain is parametrized by $\mathbf{q}_p = [y, z, \phi, q_{21}]^T$. The velocity of joints ① and ② are related to the coordinates velocities $\dot{\mathbf{q}}_p$ through the Jacobian matrices $\mathbf{J}_{p1}$ and $\mathbf{J}_{p2}$

$$\begin{bmatrix}\dot{\mathbf{r}}_1\\ \dot{\mathbf{r}}_2\end{bmatrix} = \begin{bmatrix}\mathbf{J}_{p1}\\ \mathbf{J}_{p2}\end{bmatrix}\dot{\mathbf{q}}_p = \mathbf{J}_p\dot{\mathbf{q}}_p \tag{2}$$

with $\mathbf{r}_1$ and $\mathbf{r}_2$ the respective positions of joint ① and ② in the vertical plane. $\mathbf{J}_p$ is a (4×4) matrix. The other coordinates of the flying robot are regrouped in the attitude coordinate vector $\mathbf{q}_a = [\psi, \theta, \varphi_1, \varphi_2]^T$. The translation along the axis $\mathbf{x}$ is treated separately (see section 3.3).

3. DYNAMIC MODEL

The dynamic model of a quadrotor presents a natural decoupling between the attitude and the translation dynamics (Castillo et al., 2005). This decoupling is preserved when the joint linking a rigid body and the drone is situated at the drone center of mass (CoM) as in Nguyen et al. (2015b). The decoupling is an asset making backstepping control popular for drones. Unfortunately, placing a joint at the drone CoM for the studied structure would restrict the range for joint motion to avoid collision between the passive chain and the drone. Therefore, the joints are not situated at the drone CoMs and the dynamic decoupling is not obtained directly. However, expressing the dynamic equations for the passive chain in the vertical plane separately from the dynamic associated to the other coordinates will allow finding decoupling properties.

3.1 Drone input wrenches

Each drone provides an actuation wrench composed of three moments and one thrust force whose direction is normal to the drone propellers plane. Those inputs are related to the eight propeller angular velocities squared through a bijection as in Castillo et al. (2005). The response time of the rotor dynamics is considered negligible compared to the drone and structure dynamics. The input wrenches in local frames $\mathcal{D}_1$ and $\mathcal{D}_2$ are given by

$$\begin{aligned}\mathbf{w_1} &= [0\ 0\ f_{1z}\ \tau_{1x}\ \tau_{1y}\ \tau_{1z}]^T\\ \mathbf{w_2} &= [0\ 0\ f_{2z}\ \tau_{2x}\ \tau_{2y}\ \tau_{2z}]^T\end{aligned} \tag{3}$$

3.2 Passive chain dynamic model

The passive chain motion restricted to the vertical plane $(x = 0)$ is considered. The dynamic model of the passive chain will be computed via Euler-Lagrange approach. The Lagrangian of the passive chain is defined by

$$L_p(\mathbf{q}_p, \dot{\mathbf{q}}_p) = E_p(\dot{\mathbf{q}}_p, \mathbf{q}_p) - U_p(\mathbf{q}_p) \tag{4}$$

where E_p is the kinetic energy of the passive chain and U_p its potential energy. In the vertical plane $(x = 0)$ two

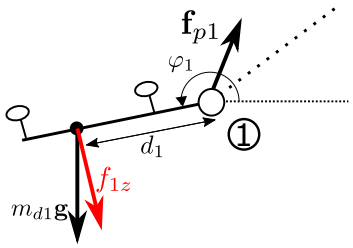

Fig. 3. Forces acting on one drone 1

planar forces $\mathbf{f}_{p1}$ and $\mathbf{f}_{p2}$ are exerted by the drones on the passive chain at respectively joints ① and ②. Euler-Lagrange equations applied to the passive chain gives

$$\frac{\mathrm{d}}{\mathrm{dt}}\left(\frac{\partial L}{\partial \dot{\mathbf{q}}_p}\right)^T - \left(\frac{\partial L}{\partial \mathbf{q}_p}\right)^T = \mathbf{J}_{p1}^T\mathbf{f}_{p1} + \mathbf{J}_{p2}^T\mathbf{f}_{p2} \tag{5}$$

with $\mathbf{J}_{p1}$ and $\mathbf{J}_{p2}$ the Jacobian matrices from (2). Using (4), equation (5) is expressed under the form

$$\mathbf{M}_p\ddot{\mathbf{q}}_p + \mathbf{c}_p = \mathbf{J}_{p1}^T\mathbf{f}_{p1} + \mathbf{J}_{p2}^T\mathbf{f}_{p2} = \mathbf{J}_p^T\begin{bmatrix}\mathbf{f}_{p1}\\ \mathbf{f}_{p2}\end{bmatrix} \tag{6}$$

with

- $\mathbf{M}_p$ the (4×4) definite positive generalized inertia matrix of the planar passive chain depending on $\mathbf{q}_p$,
- $\mathbf{c}_p$ the 4-dimensional vector of gravitational, Coriolis and centrifugal effects depending on $\mathbf{q}_p$ and $\dot{\mathbf{q}}_p$.

Away from singularities (see section 2), the Jacobian matrix $\mathbf{J}_p$ in (6) is invertible and the inverse dynamic model of the passive chain is then

$$\begin{bmatrix}\mathbf{f}_{p1}\\ \mathbf{f}_{p2}\end{bmatrix} = \mathbf{J}_p^{-T}(\mathbf{M}_p\ddot{\mathbf{q}}_p + \mathbf{c}_p) \tag{7}$$

The forces exerted by a drone on the passive chain can be linked to the drone inputs by expressing the translational dynamics of the drone i $(i = 1, 2)$ in local frame (Fig. 3)

$$\begin{bmatrix}0\\ f_{iz}\end{bmatrix} = \mathbf{R}_i\mathbf{f}_{ti} + \mathbf{p}_i \tag{8}$$

with

$$\mathbf{f}_{ti} = \mathbf{f}_{pi} + m_{di}(\ddot{\mathbf{r}}_i - \mathbf{g}) \tag{9}$$

$$\mathbf{p}_i = \begin{bmatrix}-m_{di}d_i\dot{\varphi}_i^2\\ m_{di}d_i\ddot{\varphi}_i\end{bmatrix} \tag{10}$$

and

- $\mathbf{g}$ the gravitational acceleration vector,
- d_i the distance between the joint i and the drone i CoM,
- m_{di} the mass of the drone i,
- $\mathbf{R}_i = \begin{bmatrix}\cos\varphi_i & \sin\varphi_i\\ -\sin\varphi_i & \cos\varphi_i\end{bmatrix}$ the rotation matrix about $-\varphi_i$ in the vertical plane.

Introducing (7) and (8) in (9) gives

$$\mathbf{R}_{inv}(\mathbf{\Psi}\mathbf{f} - \mathbf{p}) = \mathbf{M}_t\ddot{\mathbf{q}}_p + \mathbf{c}_t \tag{11}$$

with

$$\mathbf{R}_{inv} = \begin{bmatrix}\mathbf{R}_1^{-1} & 0\\ 0 & \mathbf{R}_2^{-1}\end{bmatrix} \quad \mathbf{\Psi} = \begin{bmatrix}0&0&0&1\\0&1&0&0\end{bmatrix}^T \quad \mathbf{p} = \begin{bmatrix}\mathbf{p}_1\\ \mathbf{p}_2\end{bmatrix}$$

$$\mathbf{c}_t = \mathbf{J}_p^{-T}\mathbf{c}_p + \begin{bmatrix}-m_{d1}l\dot{\phi}^2c_1\\ m_{d1}(-l\dot{\phi}^2s_1 + g)\\ -m_{d2}lc_2(\dot{\phi}+\dot{q}_{12})^2\\ m_{d2}(-ls_2(\dot{\phi}+\dot{q}_{12})^2 + g)\end{bmatrix}$$

$$\mathbf{M}_t = \mathbf{J}_p^{-T}\mathbf{M}_p + \begin{bmatrix}m_{d1}&0&-m_{d1}ls_1&0\\0&m_{d1}&-m_{d1}lc_1&0\\m_{d2}&0&-m_{d2}ls_2&-m_{d2}ls_2\\0&m_{d2}&-m_{d2}lc_2&-m_{d2}lc_2\end{bmatrix}$$

and $c_1 = \cos\phi$, $s_1 = \sin\phi$, $c_2 = \cos(\phi + q_{21})$, $s_2 = \sin(\phi + q_{21})$. l is the passive link length (the same for the two arms). $\mathbf{M}_t$ an invertible (4×4) matrix depending on $\mathbf{q}_p$.

The term $\mathbf{p}_i$ in (8) generates a coupling between the passive chain dynamics and the drone dynamics. In the objective of designing a cascaded controller, this term will be considered as a perturbation of the passive chain dynamics. Then, the dynamic equations of the passive kinematic chain depends only on the input thrust forces (f_{1z} and f_{2z}) and the drone roll coordinates (φ_1 and φ_2). This decoupling allows to consider the attitude coordinates as auxiliary inputs for those dynamics and lead to the control law established in section 4.

3.3 Attitude dynamic model

The dynamics of the attitude coordinates $\mathbf{q}_a = [\psi, \theta, \varphi_1, \varphi_2]^T$ is now studied. Let us now consider the Lagrangian of the *complete robot*

$$L(\mathbf{q}, \dot{\mathbf{q}}) = E(\dot{\mathbf{q}}, \mathbf{q}) - U(\mathbf{q}) \tag{12}$$

where E is the kinetic energy of the robot and U its potential energy. Euler-Lagrange equations applied to the robot gives

$$\frac{\mathrm{d}}{\mathrm{dt}}\left(\frac{\partial L}{\partial \dot{\mathbf{q}}}\right)^T - \left(\frac{\partial L}{\partial \mathbf{q}}\right)^T = \mathbf{J}^T\begin{bmatrix}\mathbf{w}_1\\ \mathbf{w}_2\end{bmatrix} \tag{13}$$

with $\mathbf{J}$ the Jacobian matrice from (1). Using (12), (13) is expressed under the form

$$\mathbf{M}\ddot{\mathbf{q}} + \mathbf{c} = \mathbf{J}^T\begin{bmatrix}\mathbf{w}_1\\ \mathbf{w}_2\end{bmatrix} \tag{14}$$

with

- $\mathbf{M}$ the (9×9) definite positive generalized inertia matrix of the structure,
- $\mathbf{c}$ the 9-dimensional vector of gravitational, Coriolis and centrifugal effects.

The direct dynamic model of the complete structure is then obtained by inverting $\mathbf{M}$ in (14)

$$\ddot{\mathbf{q}} = \mathbf{M}^{-1}\left(\mathbf{J}^T\begin{bmatrix}\mathbf{w}_1\\ \mathbf{w}_2\end{bmatrix} - \mathbf{c}\right) \tag{15}$$

The acceleration of the attitude coordinates is selected in equation (15)

$$\ddot{\mathbf{q}}_a = \mathbf{M}_{inv,a}\left(\mathbf{J}^T\begin{bmatrix}\mathbf{w}_1\\ \mathbf{w}_2\end{bmatrix} - \mathbf{c}\right) \tag{16}$$

where $\mathbf{M}_{inv,a}$ corresponds to the rows of the inverse of the matrix $\mathbf{M}$ restricted to the attitude coordinates. Introducing (3) in (16), the wrenches are expressed as function of drones input torques $\boldsymbol{\tau} = [\tau_{1x}, \tau_{1y}, \tau_{1z}, \tau_{2x}, \tau_{2y}, \tau_{2z}]^T$ and drone input forces $\mathbf{f} = [f_{1z}, f_{2z}]^T$ giving

$$\begin{aligned}\ddot{\mathbf{q}}_a &= \mathbf{M}_{inv,a}\left(\mathbf{J}_\tau^T\boldsymbol{\tau} + \mathbf{J}_f^T\mathbf{f} - \mathbf{c}\right)\\ &= \mathbf{A}_\tau\boldsymbol{\tau} + \mathbf{M}_{inv,a}\left(\mathbf{J}_f^T\mathbf{f} - \mathbf{c}\right)\end{aligned} \tag{17}$$

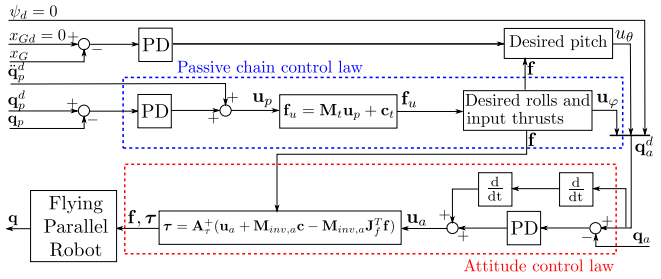

Fig. 4. General scheme of the controller

with $\mathbf{J}_\tau^T$ and $\mathbf{J}_f^T$ the columns of the Jacobian $\mathbf{J}^T$ restricted to the input torques $\boldsymbol{\tau}$ and forces $\mathbf{f}$ respectively. The matrix $\mathbf{A}_\tau$ is a (4×6) matrix linking the attitude coordinates to the input torques. This matrix has the property to remain full rank in all configurations, allowing the feedback linearization of the attitude loop realized in section 4.3. Six torque inputs are available to generate four attitude angles. This is due to the fact that over-constraints are generated by the input moments of both drones about $\mathbf{y}$ and $\mathbf{z}$ axis. Those moments are acting along the same axis and are completely transmitted through the revolute joints of the passive structure. Then, several combinations of those input torques can generate the same acceleration on the attitude variables.

3.4 Planar motion and normal-to-plane dynamics

To maintain the vertical position of the structure, the dynamics of the system in the direction $\mathbf{x}$ is expressed. Considering $\psi = 0$ and $|\theta| << 1$ the dynamic translation of the CoM of the flying structure is given by

$$\begin{aligned} m_t\ddot{x}_G &= sin(\theta)(\cos\varphi_1 f_{1z} + \cos\varphi_2 f_{2z}) \\ &\simeq \theta(\cos\varphi_1 f_{1z} + \cos\varphi_2 f_{2z}) \end{aligned} \tag{18}$$

where m_t is the total mass of the robot and x_G is its CoM position along axis $\mathbf{x}$.

4. CONTROL LAW

The control law designed for the flying robot is based on nonlinear feedback linearization already applied on classic quadrotors (Voos, 2009). The control strategy will be the combination of two cascaded loops. A slow loop is dedicated to the trajectory tracking of the passive chain coordinates. The control inputs for this loop are the drone thrust forces and the desired attitude coordinates. Then a fast control loop ensures the convergence of the robot attitude coordinates toward the desired ones. A feedback linearization is applied in each loop and time scale separation of the two loops is ensured. An additional corrective term is also implemented to maintain the structure in the vertical plane $x = 0$. Controller scheme is shown in Fig. 4

4.1 Lateral control law

From (18), θ can be used as an auxiliary input to maintain the CoM of the flying robot on the vertical plane $x_G = 0$. The desired angle is chosen in order to obtain the closed-loop equation

$$\ddot{x}_G + k_{px}x_G + k_{dx}\dot{x}_G = 0 \tag{19}$$

with gains $k_{px} > 0$ and $k_{dx} > 0$. Identifying (18) with the desired system closed-loop equation (19) gives the desired auxiliary input for θ

$$u_\theta = \frac{-k_{px}x_G - k_{dx}\dot{x}_G}{m_t(\cos\varphi_1 f_{1z} + \cos\varphi_2 f_{2z})} \tag{20}$$

The input thrust in (20) are those obtained in the computation of the passive chain control law (22). In order that the hypothesis of the flying robot maintained on a vertical plane remains valid, the gains k_{px} and k_{dx} are chosen sufficiently low. Then, the variations of the angular acceleration $\ddot{\theta}$ will not affect the dynamic model established for the passive chain. This control law is not established for tracking purpose but just to counter small perturbations along the direction $\mathbf{x}$.

4.2 Passive chain control law

Consider a desired trajectory for the passive chain coordinates $\mathbf{q}_p^d$. Consider an auxiliary control $\mathbf{u}_p$ corresponding to those coordinate accelerations. A PD control law is defined for this auxiliary input

$$\mathbf{u}_p = \ddot{\mathbf{q}}_p^d - \mathbf{K}_{pp}\mathbf{e}_p - \mathbf{K}_{dp}\dot{\mathbf{e}}_p \tag{21}$$

with

- $\mathbf{e}_p = \mathbf{q}_p - \mathbf{q}_p^d$ the position tracking error,
- $\mathbf{K}_{pp}$ and $\mathbf{K}_{pd}$ two definite positive matrices.

Ignoring the perturbation term $\mathbf{p}$, from (11) the drone input thrust forces $\mathbf{f} = [f_{1z}, f_{2z}]^T$ required to produce the desired auxiliary inputs $\mathbf{u}_p$ are computed by

$$\begin{aligned} \mathbf{f} &= \begin{bmatrix} -\sin\varphi_1 & \cos\varphi_1 & 0 & 0 \\ 0 & 0 & -\sin\varphi_2 & \cos\varphi_2 \end{bmatrix} \begin{bmatrix} \mathbf{f}_{u1} \\ \mathbf{f}_{u2} \end{bmatrix} \\ \begin{bmatrix} \mathbf{f}_{u1} \\ \mathbf{f}_{u2} \end{bmatrix} &= \mathbf{M}_t\mathbf{u}_p + \mathbf{c}_t \end{aligned} \tag{22}$$

The closed-loop equation of the passive chain is obtained by applying the computed input forces (22) to its dynamic model (11).

$$(\mathbf{M}_t\mathbf{u}_p + \mathbf{c}_t) - \boldsymbol{\delta} - \mathbf{R}_{inv}\mathbf{p} = \mathbf{M}_t\ddot{\mathbf{q}}_p + \mathbf{c}_t \tag{23}$$

where

$$\boldsymbol{\delta} = \mathbf{R}_{inv} \begin{bmatrix} f_{u1y}\cos\varphi_1 + f_{u1z}\sin\varphi_1 \\ 0 \\ f_{u2y}\cos\varphi_2 + f_{u2z}\sin\varphi_2 \\ 0 \end{bmatrix} \tag{24}$$

is a perturbation term due to the drones underactuation. The term $\boldsymbol{\delta}$ can be canceled by choosing appropriate drone roll angles. Two auxiliary inputs u_{φ_i} corresponding the drone roll angles are defined

$$u_{\varphi_i} = \text{atan2}(f_{uiy}, -f_{uiz}) \tag{25}$$

From (24) and (25), we have $\boldsymbol{\delta} \to \mathbf{0}$ when $\varphi_i \to u_{\varphi_i}$ for $i = 1, 2$. $\mathbf{M}_t$ being an invertible matrix, the closed loop-equation obtained by introducing (21) in (23) is

$$\ddot{\mathbf{e}}_p + \mathbf{K}_{pp}\mathbf{e}_p + \mathbf{K}_{dp}\dot{\mathbf{e}}_p + \mathbf{M}_t^{-1}(\boldsymbol{\delta} + \boldsymbol{\delta}_p) = \mathbf{0} \tag{26}$$

The perturbation $\boldsymbol{\delta}_p = \mathbf{R}_{inv}\mathbf{p}$ associated to the drones angular velocities and accelerations will be treated in section 4.4. Considering this perturbation negligible, the attitude loop will be controlled to make each drone roll angle φ_i converge toward the desired input value u_{φ_i}. Then, the closed-loop of the passive chain behaves as a secondary ordinary differentiation equation ensuring the convergence of $\mathbf{e}_p$ and $\dot{\mathbf{e}}_p$ towards zero.

4.3 Attitude control law

Similarly to the passive chain control loop, the attitude control loop uses dynamic inversion to converge toward the desired configuration. The desired configuration vector $\mathbf{q}_a^d$ is contains the terms

- $\psi^d = 0$ to maintain the robot on its vertical plane,
- u_θ from (20) to generate the correction along the direction $\mathbf{x}$,
- u_{φ_1} and u_{φ_2} from (25) to obtain the convergence on the passive chain loop.

Through dynamic inversion, a PD control law is designed on the auxiliary input $\ddot{\mathbf{q}}_a$

$$\mathbf{u}_a = \ddot{\mathbf{q}}_a^d - \mathbf{K}_{pa}\mathbf{e}_a - \mathbf{K}_{da}\dot{\mathbf{e}}_a \tag{27}$$

with $\mathbf{e}_a = \mathbf{q}_a - \mathbf{q}_a^d$ the position tracking error and $\mathbf{K}_{pa}$ and $\mathbf{K}_{da}$ two definite positive matrices. Taking into account the over-actuation discussed in section 3.3, the input torques $\boldsymbol{\tau}$ are then computed with (17)

$$\boldsymbol{\tau} = \mathbf{A}_\tau^+(\mathbf{u}_a + \mathbf{M}_{inv,a}\mathbf{c} - \mathbf{M}_{inv,a}\mathbf{J}_f^T\mathbf{f}) \tag{28}$$

with $\mathbf{f}$ the input thrust vector issued from (22). Using the pseudo-inverse $\mathbf{A}_\tau^+$, the solution minimizing the input torques norm is chosen among the possible solutions. As the inputs, $\mathbf{f}, \boldsymbol{\tau}$ are applied to the robot, the attitude closed-loop converges as a second order ode.

4.4 Perturbation handling

A perturbation term $\boldsymbol{\delta}_p$ has been identified in the closed-loop equation of the passive structure control (26). From equation (8), this perturbation can be partly rejected by replacing f_{iz} the thrust inputs computed in equation (22)

$$\mathbf{f} = \begin{bmatrix} -\sin\varphi_1 & \cos\varphi_1 & 0 & 0 \\ 0 & 0 & -\sin\varphi_2 & \cos\varphi_2 \end{bmatrix} \begin{bmatrix} \mathbf{f}_{u1} \\ \mathbf{f}_{u2} \end{bmatrix} + \begin{bmatrix} m_{d1} d_1 \ddot{\varphi}_1 \\ m_{d2} d_2 \ddot{\varphi}_2 \end{bmatrix} \tag{29}$$

In this case, the perturbation term becomes

$$\boldsymbol{\delta}_p = \mathbf{R}_{inv} \begin{bmatrix} -m_{di} d_1 \dot{\varphi}_1^2 & 0 & -m_{di} d_2 \dot{\varphi}_2^2 & 0 \end{bmatrix}^T \tag{30}$$

The perturbation associated to the drone acceleration have been rejected. This modification of the thrust input forces do not impact the attitude loop. The remaining perturbation $\boldsymbol{\delta}_p$ that could not be rejected converges toward zero as the drone angular velocity converges toward zero. In static equilibrium, simulations showed that this term does not impact the stability. However, it affects the tracking performance for fast motions.

5. SIMULATIONS

5.1 Simulation design

A simulator was designed using MATLAB-SIMULINK and ADAMS co-simulation. The flying structure dynamic simulation was ensured by ADAMS while the control loop was implemented on SIMULINK. A discrete communication time (1 kHz) is set between the two software to represent the measurement sampling. The simulator considers that the coordinate vector $\mathbf{q}$ is fully measured. Such measures could be obtained on a real prototype using a vision-based pose estimation as in Achtelik et al. (2009) and encoders on passive joints.

To test the robustness of the controller against noisy pose estimation, a uniformly distributed noise was added to each variables of the pose estimation and encoder resolution was also taken into account. The interval of the uniform distribution in the simulation results presented is $\left[-1e^{-3}; 1e^{-3}\right]$ rad for the orientation coordinate estimations and $\left[-1e^{-3}; 1e^{-3}\right]$ m for the position estimations. The robustness of the controller was observed with noise range up to $\left[-1e^{-2}; 1e^{-2}\right]$. As the feedback linearizations lead to equivalent second order ordinary differential equations, the PD gains were set to ensure a unitary relative dampling. The tuning parameter is then the natural pulsation ω_n leading to proportional gain ω_n^2 and derivative gain $2\omega_n$. The natural pulsation selected for each controlled coordinate are for drone roll: 20 rad/s, for attitude (ψ, θ): 7 rad/s, for the passive chain coordinates: 3 rad/s, for lateral control: 2 rad/s. The natural pulsation associated the variables used to maintain the flying structure in a vertical plane are voluntary chosen low to limit perturbations over the dynamic model of the passive chain. The gains are also selected to ensure a time scale separation between the loops. The time derivatives of the desired configuration $\mathbf{q}_a^d$ for the attitude loop are numerically computed and filtered with lowpass Butterworth filters.

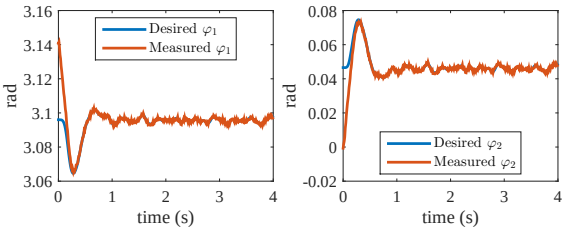

Fig. 5. Convergence on drone roll angles

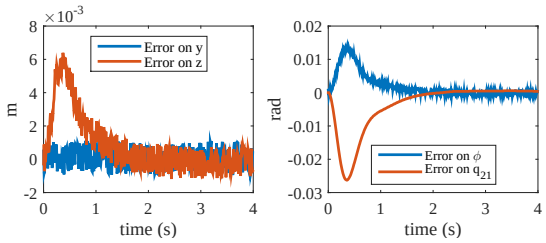

Fig. 6. Stabilization of the passive kinematic chain from an unstable initial position

5.2 Stabilization

A first simulation shows the stabilization of the flying structure from an initial position. The structure is placed in an unstable initial position as in Fig. 1. The two drones are in a horizontal position. As the drones cannot compensate the lateral forces generated by the passive chain, the position is unstable. With a constant input on the passive chain desired position, the controller will drive the drones angles to a constant position assuring the stabilization of the structure. Fig. 5 shows the desired drone roll angles and the convergence toward those desired angles. Fig. 6 shows the error obtained on the passive kinematic chain parameters $\mathbf{q}_p$. As the initial position is not stable, those parameters diverge from their initial position but are driven back by the controller when the convergence is obtained on the attitude loop.

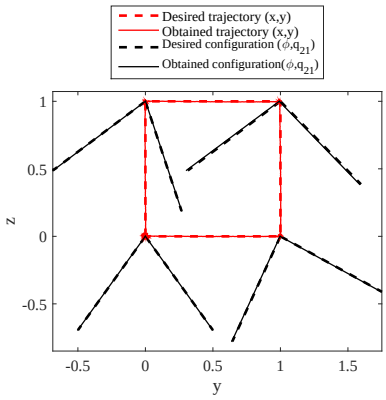

Fig. 7. Desired and obtained motion for $t_e = 3$ s

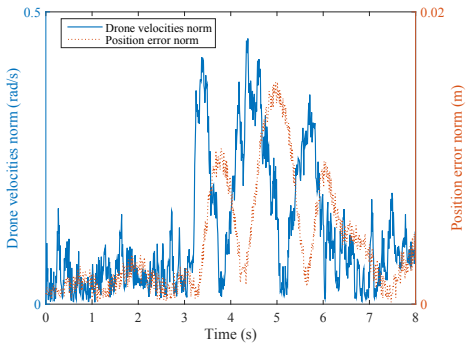

Fig. 8. Influence of the drone velocity over tracking error

5.3 Trajectory tracking

From a stabilized position, a square trajectory was designed in the plane ($x = 0$). At each corner of the square, different angles ϕ and q_{21} are desired on the passive chain. The trajectory and its first to forth time derivatives are designed to be continuous on all controlled variables. The desired duration for the robot to travel each edge of the square is defined by the time t_e. Fig. 7 shows the desired trajectory and obtained trajectory with $t_e = 3$ s. In simulation, the controller shows good performances in maintaining the passive chain on the desired trajectory and remains robust against noisy measures. Figure 8 compares the evolution of the position tracking error and drone angular velocity along the trajectory. The perturbation term associated to the drone angular velocity clearly impact the trajectory tracking precision, with phase shift as it acts on the passive structure acceleration. Nevertheless, it remains sufficiently low to not affect the controller stability. The inputs wrenches (3) are linearly related to the force provided by each rotor. In this simulation, the force provided by each propeller is in range [4.8,8.5] N.

6. CONCLUSION AND FUTURE WORK

In this paper, a new type of flying parallel robot was studied. The robot is composed of two quadrotors linked by a rigid articulated passive chain, that can be assimilated to a flying parallel robot. The study of the dynamic model showed decoupling properties. Those properties have been exploited to design a controller dedicated to this new flying robot. Simulations showed the performance and the robustness against noisy pose estimation of the controller designed. The promising results obtained provide a good base for the future development of flying parallel robots. Future work on the architecture presented in this paper includes the design of optimal trajectories with respect to the drones payload; the consideration of the impact of the drone centrifugal force to avoid unstability and to increase accuracy; application of reconfiguration techniques known for parallel robots on the flying robot; design of a position/force controller to interact with the environment. Such technique will allow positioning the tool tip over or under the drones, in function of the task objective. A prototype of the robot is also under construction to test the controller developed in a real environment.

REFERENCES

Achtelik, M., Zhang, T., Kuhnlenz, K., and Buss, M. (2009). Visual tracking and control of a quadcopter using a stereo camera system and inertial sensors. In *International Conference on Mechatronics and Automation*, 2863–2869. Changchun, China.

Castillo, P., Lozano, R., and Dzul, A. (2005). Stabilization of a mini rotorcraft with four rotors: Experimental implementation of linear and nonlinear control laws. *IEEE Control Systems Magazine*, 25(6), 45–55.

Gogu, G. (2008). *Structural synthesis of parallel robots*. Springer edition.

Gosselin, C. and Angeles, J. (1990). Singularity analysis of closed-loop kinematic chains. *IEEE Transactions on Robotics and Automation*, 6(3), 281–290.

Kim, S., Choi, S., Lee, H., and Kim, H.J. (2014). Vision-based collaborative lifting using quadrotor UAVs. In *International Conference on Control, Automation and Systems*, Oct, 1169–1174. Seoul, Korea.

Korpela, C., Orsag, M., Pekala, M., and Oh, P. (2013). Dynamic stability of a mobile manipulating unmanned aerial vehicle. In *IEEE International Conference on Robotics and Automation*, May, 4922–4927. Karlsruhe, Germany.

Manubens, M., Devaurs, D., Ros, L., and Cortés, J. (2013). Motion Planning for 6-D Manipulation with Aerial Towed-cable Systems. In *Robotics: Science and Systems*, Jun. Berlin, Germany.

Nguyen, H.N., Ha, C., and Lee, D. (2015a). Mechanics, control and internal dynamics of quadrotor tool operation. *Automatica*, 61, 289–301.

Nguyen, H.N., Park, S., and Lee, D. (2015b). Aerial tool operation system using quadrotors as Rotating Thrust Generators. In *International Conference on Intelligent Robots and Systems*, Sep, 1285–1291. Hamburg, Germany.

Sreenath, K. and Kumar, V. (2013). Dynamics, Control and Planning for Cooperative Manipulation of Payloads Suspended by Cables from Multiple Quadrotor Robots. In *Robotics: Science and Systems*, May. Berlin, Germany.

Voos, H. (2009). Nonlinear control of a quadrotor micro-uav using feedback-linearization. In *IEEE 2009 International Conference on Mechatronics*, Apr. Malaga, Spain.

Yang, H. and Lee, D. (2014). Dynamics and Control of Quadrotor with Robotic Manipulator. In *International Conference on Robotics and Automation*, May, 5544–5549. Hong Kong, China.